Honeycomb Cell Structures Formed in Drop-Casting CNT Films for Highly Efficient Solar Absorber Applications

Saiful Islam * and Hiroshi Furuta *

Posted Date: 25 September 2024

doi: 10.20944/preprints202409.1955.v1

Keywords: solar absorber; spectral selectivity; Honeycomb structure; drop casting technique; CNTs; solar radiation intensity

Article

Honeycomb Cell Structures Formed in Drop-Casting CNT Films for Highly Efficient Solar Absorber Applications

Saiful Islam [1,2,*] and Hiroshi Furuta [1,2,*]

[1] School of Systems Engineering, Kochi University of Technology, Kochi 782-8502, Japan
[2] Center for Nanotechnology, Research Institute, Kochi University of Technology, Kochi 782-8502, Japan
* Correspondence: md.saiful38@gmail.com (S.I.); furuta.hiroshi@kochi-tech.ac.jp (H.F.); Tel.: +81-887531111. (S.I.) , +81-887572211. (H.F.)
† This paper is an extended version of our conference proceedings at the 14th International Conference on Metamaterials, Photonic Crystals and Plasmonics., Toyama, Japan, July 16 – 19, 2024.

Abstract: This study investigates the process of multi-walled carbon nanotube (MWCNT) coatings to enhance the lamp heating temperature for solar thermal absorption applications. The primary focus is studying the effects of self-organized honeycomb structures of CNTs formed on silicon substrates on different cell area ratios (CAR). The drop-casting process developed honeycomb-structured MWCNT-coated absorbers with varying CAR values ranging from ~ 60% to 17%. The optical properties were investigated within the visible (400-800 nm) and near-infrared (934-1651nm) wavelength ranges. Although fully coated MWCNT absorbers showed the lowest reflectance, honeycomb structures with a ~ 17% CAR achieved high-temperature absorption. These structures maintained 8.4% reflectance at 550 nm while dramatically increasing infrared reflection to 80.5% at 1321 nm. The performance of solar thermal was assessed throughout a range of irradiance intensities, from 0.04 W/cm² to 0.39 W/cm². The honeycomb structure with a ~17% CAR value consistently performed better than other structures by reaching the highest absorption temperatures (ranging from 52.5°C to 285.5°C) across all measured intensities. A direct correlation was observed between the reflection ratio (visible: 550 nm / infrared: 1321 nm) and temperature absorption efficiency, where lower reflection ratios were associated with higher temperature absorption. This study highlights the significant potential for the large-scale production of cost-effective solar thermal absorbers through the application of optimized honeycomb-structured absorbers coated with MWCNTs. These contributions enhance solar energy efficiency for applications in water heating and purification, thereby promoting sustainable development.

Keywords: solar absorber; spectral selectivity; Honeycomb structure; drop casting technique; CNTs; solar radiation intensity

1. Introduction

Global development and human progress are significantly impeded by the scarcity of potable water, electricity, and heated water for domestic and industrial applications [1–3]. Solar energy is distinguished from other renewable energy sources, such as wind, geothermal heat, and hydrogen, by its reliability, accessibility, and abundance. Diverse applications, such as electricity generation, water heating, and seawater desalination, are available through solar power. Nevertheless, the thermal efficacy of solar energy systems remains suboptimal despite these advantages. A promising approach to enhancing the efficacy of solar thermal devices is enhancing the properties of solar absorption materials [4]. Hydrophilicity, porosity, self-floating properties, and high solar-thermal conversion efficiency are all essential characteristics of ideal solar absorption materials [5]. These materials are essential in nearly all solar applications, as they are the primary medium for absorbing solar energy and facilitating thermal management processes. In solar thermal applications, the absorbing material must effectively capture solar radiation and convert it to thermal energy. That

 doi:10.20944/preprints202409.1955.v

energy is then conveyed to a working fluid to increase its temperature. Carbon nanotubes (CNTs) have become highly effective solar absorbers in solar thermal systems, predominantly due to their broad absorption spectrum [6].

The extraordinary optical [7], electrical [8], and mechanical [9] properties of CNTs, which were initially documented by Sumio Iijima in 1991 [10], have since attracted significant scientific interest. The prospective applications of these distinctive characteristics in renewable energy systems have been the subject of extensive research. CNTs are distinguished as one of the darkest materials on Earth due to their exceptional light-absorbing properties [11]. This property is especially pertinent in solar thermal technology, where materials on the brink of achieving optimal black body absorption are highly desirable.

The exceptional solar absorber performance of MWCNT film provides valuable insights into the design and fabrication of optical absorption materials. The vital function of surface micro-nano structure design and preparation procedures in determining absorption performance in practical applications is underscored by the inherent absorption properties of MWCNT film [12–15]. The broadband absorption characteristics of the MWCNT absorber, which include the infrared (IR) region, contribute to increased radiation loss, even though MWCNTs exhibit high thermal conductivity and exceptional optical absorption properties [16,17].

Previous research has introduced a variety of structures, such as multilayered formations and composite absorbers, to resolve wavelength selectivity and radiation issues. This comprehension underscores the significance of modifying the structural characteristics of MWCNT film-based absorbers such as (3D wavy structure [18], peak-like structure [19], forest-like structure [20], multilayer structure [21]) to optimize their efficacy in solar absorbers. Udorn et al. [22] reported that CNT honeycomb structures, which were fabricated by short ethanol treatment durations on CNT forests (synthesized via thermal CVD, yielding ~8.0 × 10^9 CNTs/cm^2 with ~10 μm height) and having cell areas below 30 $μm^2$, wall heights around 5.5 μm, and thin buckypaper films (0.2 μm), exhibited a high total reflectance of up to 10-12% in the UV region and 6-8% in the visible region. Hong et al. [23] developed the 3D origami solar steam generator by spray coating a graphene oxide/carbon nanotube composite onto a preheated porous cellulose membrane structured with a Miura-ori tessellation. The generator achieved a surface area density of 4.65 and an evaporation rate of 1.59 kg/(m^2 h) under one sun illumination, resulting in a solar energy efficiency of nearly 100%. Kiani et al. [24] prepared the hierarchical Cu-CNT nanowire structure fabricated through copper thermal oxidation, hydrogen reduction, and self-catalytic CVD of CNTs using acetylene. The resultant structure exhibited ultra-broadband near-perfect light absorption, with an average total reflectance of 0.75% and specular reflectance of 0.1% over the 400-1000 nm wavelength range. Ghai et al. [25] synthesized flower-like carbon nanotubes (FCNTs) using a two-step thermal CVD process that involved a dual etching technique. These FCNTs demonstrated exceptional blackbody properties, with a light absorption rate of over 99.97% and an emissivity of 0.98 in the UV-Vis-NIR range. Pander et al. [26] demonstrated that The CNT Forest fishnet metamaterials, which were self-assembling and using a polystyrene nanosphere monolayer as a shadow mask during the deposition of the catalyst, showed a blueshift in broadband reflectance peak from 550 nm to 460 nm, as the size of the holes increased from 370 nm to 665 nm, attributed to changes in inductance and capacitance. Huang et al. [27] prepared the multilayered structured absorber utilizing CMP–CNT(average tube diameter of CNT -15 nm)/CNP–TiN coatings and achieved an average light absorptance of 96.4% in the 400–1400 nm wavelength range. The fabrication process involved the use of a high-voltage electrostatic spraying approach.

The thermal absorption of MWCNT-based absorbers is significantly improved under different solar intensities. It is essential to mention intensity issues because variations in solar irradiance directly influence the performance and efficiency of solar absorbers [28]. For instance, He et al. [29] prepared the PDA@CNT/PU nanofiber membrane solar steam generator, achieved high evaporation rates and solar-to-vapor conversion efficiencies of up to 1.44 kg m^{-2} h^{-1} and 90.1% under one sun illumination, exhibiting excellent anti-oil-fouling ability and stability even with oil-contaminated water. Jin et al. [30] reported that the CNT-RGO@BC composite absorber exhibited efficient solar interface evaporation, as evidenced by its high photothermal conversion efficiency of 90.2% and an evaporation rate of 1.85 kg m^{-2} h^{-1} under one solar irradiation. Li et al. [31] demonstrated that the porous Ni/CNTs composite membrane, which was employed as a highly efficient solar

 doi:10.20944/preprints202409.1955.v

absorber, achieved an impressive solar energy utilization rate of 94.3% and an evaporation rate of 2.13 kg m^{-2} h^{-1} under one sun irradiation, with a radiation loss of 1.6%. Zhang et al. [32] introduced a spray-based method for the bulk production of GO/CNT-based solar evaporator membranes. They utilized a tunnel to dry the membrane evaporator continuously. They achieved inadequate efficiency as the sun's intensity increased due to heat losses. Wang et al. [33] introduced the hanging-mode solar evaporator, which utilized a polyaniline/carbon nanotube (PANI/CNT) composite absorber and obtained a photothermal efficiency of 91.74% and an evaporation rate of 2.81 $kg \cdot m^{-2} \cdot h^{-1}$ under one solar illumination.

Despite their promising features, the widespread adoption of MWCNT coatings in scalable applications is hindered by numerous inherent limitations. The fabrication methods for MWCNTs are relatively complex, frequently necessitating subsequent transfer processes and typically involving chemical vapor deposition (CVD) techniques. These procedures are mainly restricted to small-scale processes, substantially hindering the broader implementation and scale-up of MWCNT-based absorbers [34,35]. Additionally, MWCNT composite absorbers process high-cost and complex preparation procedures for large-scale fabrication. Furthermore, most experiments have been conducted in environments with 0.1W/cm^2 of sunlight (1 sun). However, more than this illumination level is required for practical applications due to the variation in solar irradiance from one region to another, which is influenced by the weather and climate. The actual applications of solar thermal devices in environments with low (< 0.1 W/cm^2) and high (> 0.1 W/cm^2) radiation have substantial effects [36,37].

In this paper, the relationship between the self-organized honeycomb-structured MWCNT absorbers and the optical and thermal properties of MWCNT honeycombs is reported. This investigation introduces a simple method for fabricating randomly aligned MWCNT honeycombs. MWCNT honeycomb structures with different cell areas and fully coated areas are presented. Subsequently, the reflectance of different cell areas of honeycomb structures composed of MWCNT was studied. Furthermore, the thermal performance of MWCNT honeycomb structures under different lamp intensities was evaluated. These findings are considered in the context of potential applications in solar thermal devices.

2. Methods

2.1. Materials

Randomly aligned multi-walled carbon nanotubes (MWCNTs) (5 wt%) dispersed in ethanol solvent (Product name: MW-I) were purchased from Meijo Nanocarbon Co., Ltd. (Tokyo, Japan). The MWCNTs had a diameter ranging from 10-40 nm [38]. Ethanol (99.5% purity) was purchased from Wako Pure Chemical Industries, Ltd. (Osaka, Japan) and used without further purification.

2.2. Preparation of MWCNTs Absorber

A fixed volume of 25.0 µL of dispersed MWCNT was used for each sample preparation. Ethanol (EtOH) volumes ranged from 25 µL to 1000 µL. The range of concentrations was set as 25 µL for EtOH volumes ranging from 25 µL to 100 µL and 100 µL for EtOH volumes ranging from 100 µL to 1000 µL. To ensure homogeneity, a set volume of MWCNT solution and EtOH were combined and stirred for 2 minutes for each sample. The thermally oxidized Si (th-SiO) substrates with resistivity of ≥ 100 Ω.cm were cut manually into 1 cm x 1 cm x 0.0525 ± 0.0025 cm using the diamond cutter and coated with 4.0 ± 0.5 µL of the prepared MWCNT/EtOH mixture using a drop-casting technique. The samples were subsequently placed inside the chamber for ~ 4 hours to allow the EtOH solvent to evaporate at ~25 °C and ~50% humidity. The bottom area of the chamber was covered by wet tissue to maintain the humidity at ~ 50%. Following this, each sample was subjected to a thermal treatment at 300°C for 1 hour to eliminate residual solvents and organic components. The heated samples were then placed into the chamber to reach the temperature at 25°C. The comprehensive procedure for preparing MWCNT-based absorbers is illustrated in Figure 1.

 doi:10.20944/preprints202409.1955.v

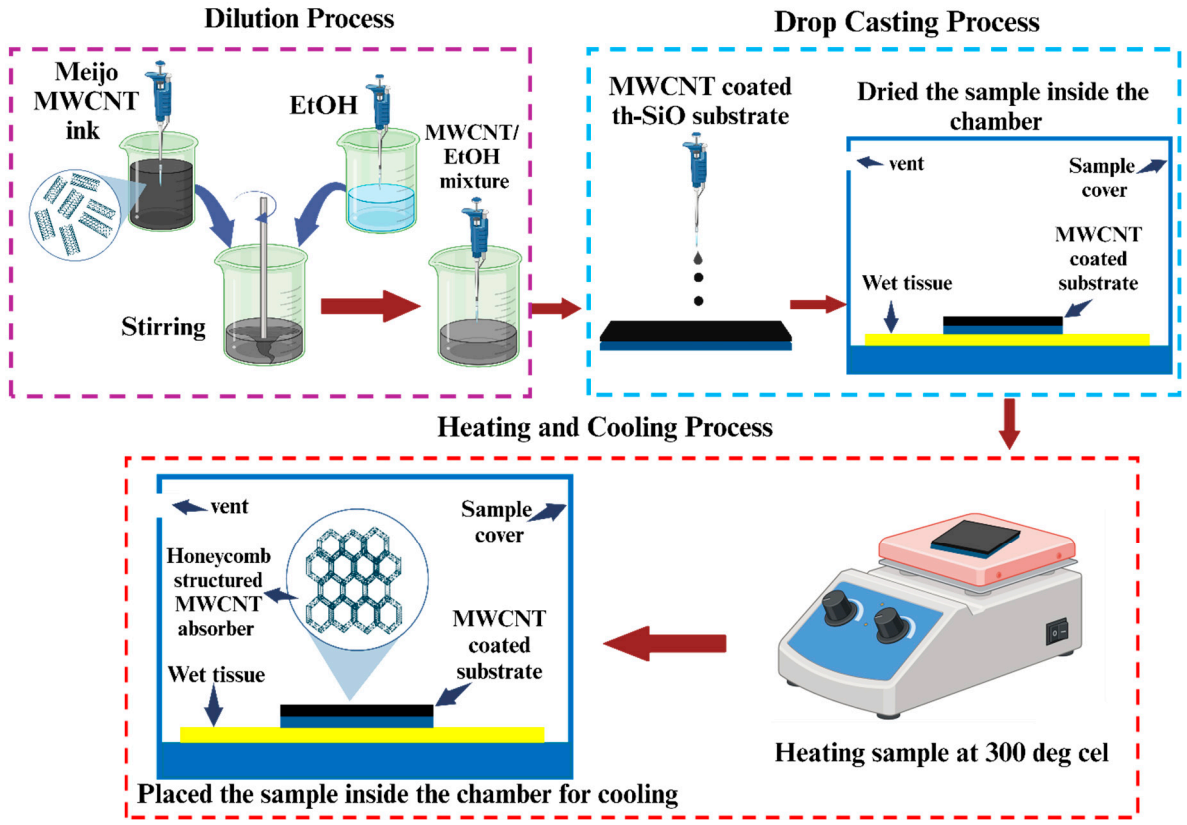

Figure 1. Detailed procedures for preparing MWCNT-coated absorbers.

2.3. Optical Measurements

A UV-vis spectrophotometer (HITACHI U-3900, HITACHI high-technologies, Tokyo, Japan) provided with an integrating sphere was employed to measure the reflectance in the UV-visible wavelength region within the range of 190-900 nm. An optical spectrometer (USB2000+, Ocean Optics, USA) was deployed to measure specular reflectance in the visible range from 400 nm to 800 nm, using a 45-degree incidence angle. An IR spectrometer (FLAME NIR, Ocean Optics, USA) was employed to measure reflectance in the near-infrared region from 934 nm to 1651 nm. The NIR spectrometer was equipped with a tungsten halogen light (HL-2000-HP, Ocean Optics, USA) and a fiber optic holder (RPH-SMA, Thorlabs, USA) to detect reflectance in the near-infrared (NIR) range. The absorption spectrum was derived from the reflectance values using the following equation:

$$A + R + \gamma = 1 \quad \textbf{(1)}$$

Here, A= Absorptance, R=Reflectance, γ =Transmittance.

2.4. Thermal Measurements

The laboratory-scale experiment employed a halogen lamp with a 10 mm beam diameter focusing mirror as an alternative source of simulated solar heat. The MWCNT-coated sample was positioned below the heater at a varying distance of ~ 40 and ~ 70 mm. A Kapton tape was attached to the rear side of the sample to monitor the output temperature using an infrared camera (FLIR Ax5 camera), as shown in Figure 2. Power levels of 26 W, 48 W, and 78 W were applied via an autotransformer to investigate the MWCNT-coated absorber's temperature response to different power intensities of irradiation. The lamp intensities were calculated using Eq. 2, which expresses the relationship between intensity (I), power (P), and distance (D) as,

$$I = \frac{P}{4\pi D^2} \quad (2)$$

 doi:10.20944/preprints202409.1955.v

The intensities implemented in these experiments were 0.04, 0.08, 0.13, 0.24, and 0.39 W/cm², as determined by Eq. 2. In this paper, we defined low intensities conditions as less than 0.1 W/cm², equivalent to 1 Sun.

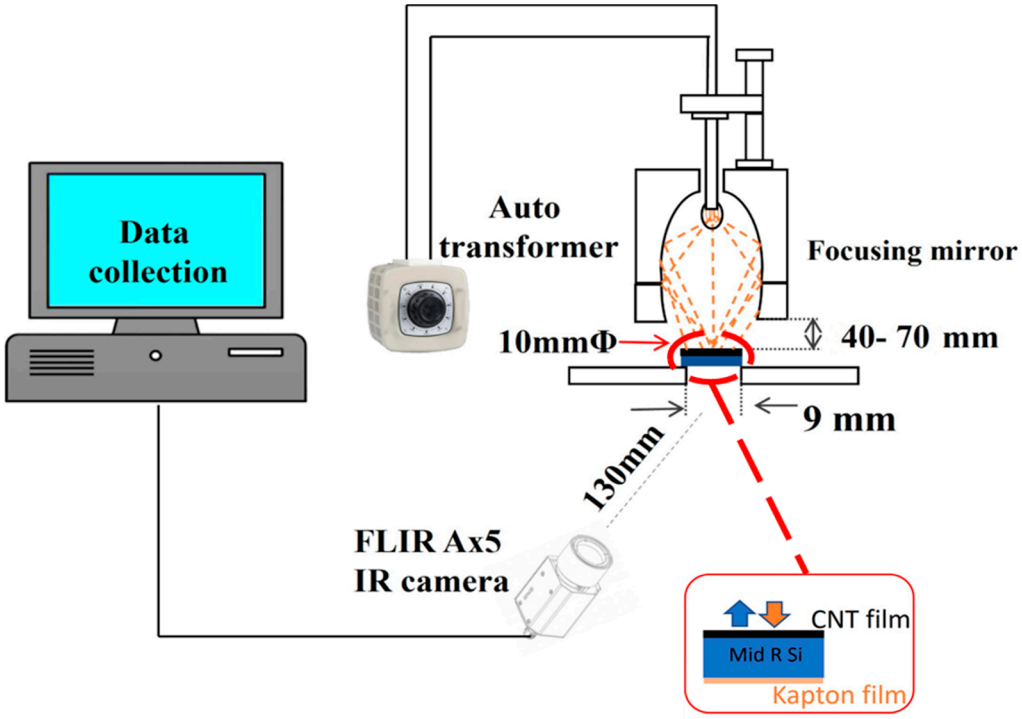

Figure 2. Experimental setup for lamp heating experiment of MWCNT coated absorber under different intensities.

3. Results and Discussion

3.1. Cell Area Analysis

The self-organized honeycomb-like structures formed by the MWCNTs are shown in Figure 3 (a-c). These structures are characterized by the interconnected networks of MWCNTs surrounded by pore areas. The wrinkles were formed during the thermal treatment of the MWCNT film at 300 °C to produce honeycomb structures. The formation of these wrinkles on the films results in the evaporation of the solvent [39,40].

Cell area ratio (CAR) is an essential parameter that quantifies the ratio of pore area to the total surface area of the self-organized honeycomb structured MWCNTs film. Figure 3(d) shows that the S11 sample is fully covered by MWCNT film with 0% CAR. A higher CAR indicates a more open structure with larger cells, whereas a lower CAR denotes a more compact network with smaller cells. The CAR values for each sample (S1, S7, and S10) indicate that a reduction in ethanol content leads to a decrease in CAR, as shown in Figure 3(a-c).

The graph in Figure 3(e) clearly represents the correlation between the amount of ethanol and the cell area ratio for each sample. As the ethanol concentration increases from 100 µL to 1000 µL, the cell area ratio increases from around ~ 17% to 60%. The observed pattern indicates that ethanol substantially influences the density, alignment, and porousness of the self-arranged honeycomb structured multi-walled carbon nanotubes (MWCNT) film. The cell area ratio for S11-S13 is none, as no honeycomb structure is formed by decreasing the ethanol concentration below 100 µL.

 doi:10.20944/preprints202409.1955.v

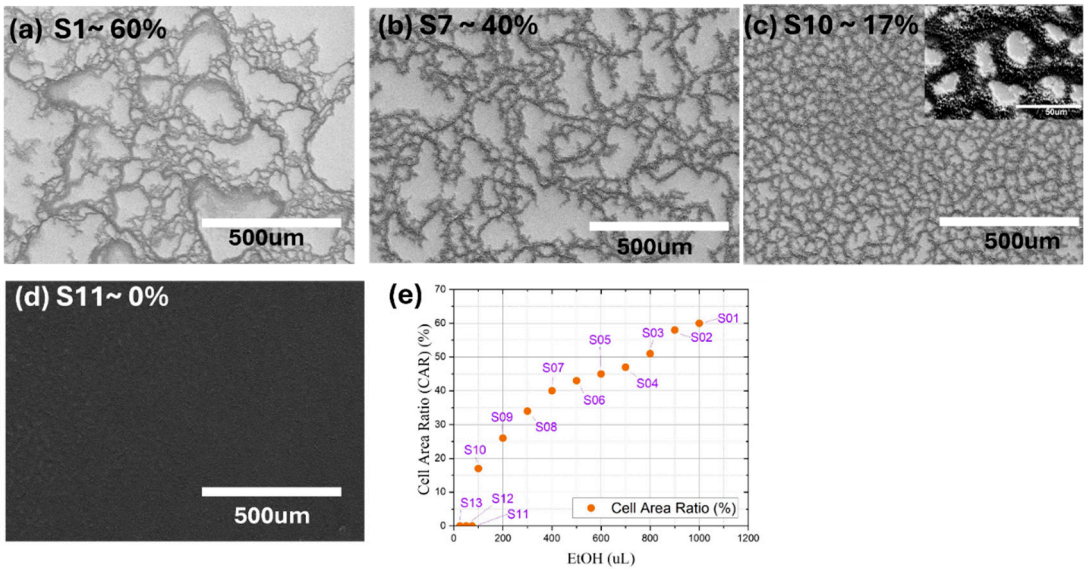

Figure 3. Effect of ethanol content on cell area ratio and morphology of MWCNT honeycomb structures. (a-c) FESEM images of the top surface of MWCNT honeycomb structures for (a) S1(CAR ~ 60%), (b) S7 (CAR~ 40%), (c) S10 (CAR~ 17%), (d) S11 (CAR-0%). (e) The correlation between the ethanol (EtOH) amount utilized in the deposition process and the cell area ratio (%).

Raman spectroscopy was employed to further characterize the deposited MWCNT-coated samples. The Raman spectra of the top surface of S01, S07, S10, and S11 samples are depicted in Figure 4(a). Furthermore, Figure 4(b) illustrates the Raman spectra of the S11 sample's top surface and sidewall. The typical silicon peak was observed at 520 cm^{-1} for the S01 sample, suggesting that the MWCNT film is not densely packed on the substrate. The G band was consistently observed at 1575 cm^{-1} and the 2D band at 2750 cm^{-1} for all samples, including the sidewall of the S11 sample in Figure 4(b), while the D band of MWCNTs was consistently observed at 1345 cm^{-1} in Figure 4(b). Radial breathing modes (RBM) were absent in the spectra. These spectroscopic results further demonstrate that the S11 sample exhibits a complete coverage of the MWCNT film, as evidenced by the presence of a peak in the sidewall spectrum in Figure 4(b), and confirm the presence of MWCNTs on the substrate.

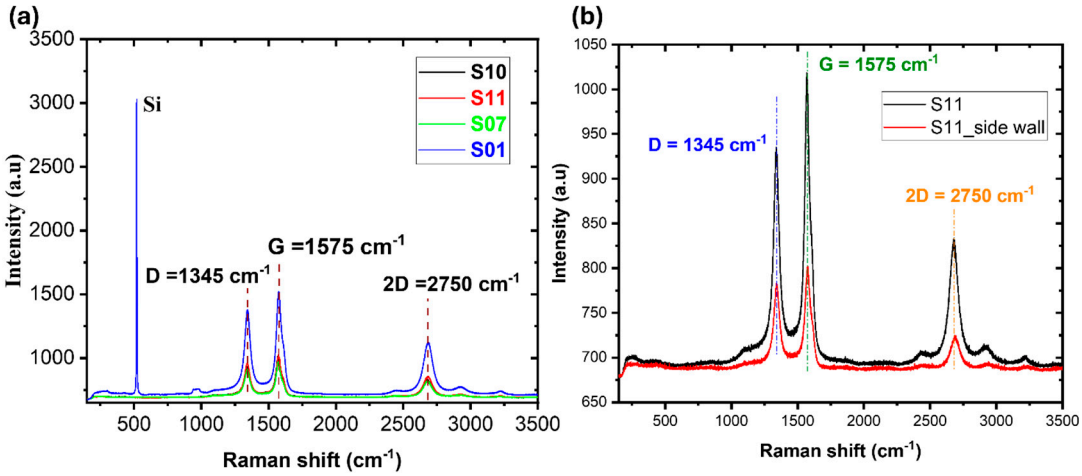

Figure 4. Raman spectra of MWCNT coated absorbers on (a) top surfaces of S01, S07, S10, and S11, and (b) top surface and side wall of fully coated MWCNT absorber of S11.

3.2. Optical Analysis

Specular reflectance was measured in the visible spectrum from 400 nm to 800 nm using a Visible spectrometer (USB2000+, Ocean Optics, USA) with a 45-degree incidence angle. Figure 5(a) illustrates the reflection patterns of MWCNT-coated samples with different cell area ratios (CAR), specifically

 doi:10.20944/preprints202409.1955.v

S01, S07, S10, and S11. The substrate S11, which was entirely covered with MWCNT and had no CAR, demonstrated the lowest throughout the observed wavelength range.

Figure 5(b) provides each sample's reflectance values at 550 nm to investigate reflection in the peak solar intensity wavelength range (490-580 nm). The absorber coated with fully covered MWCNT, designated as S13, had the lowest reflection at a wavelength of 550 nm, with a reflectance of 3.3 ± 0.5%. The honeycomb-formed MWCNT absorber with the lower CAR, S10, achieved a reflection rate of 8.4 ± 0.8% at this specific wavelength. The honeycomb-structured MWCNT absorber, designated as S01, with a higher CAR, demonstrated a reflection efficiency of 16.5 ± 0.8% at a wavelength of 550 nm. The findings indicate that thoroughly coating the MWCNT layer resulted in the lowest reflection level across the spectrum. However, the lower CAR still achieved a relatively low reflection level in a vital region of the solar spectrum.

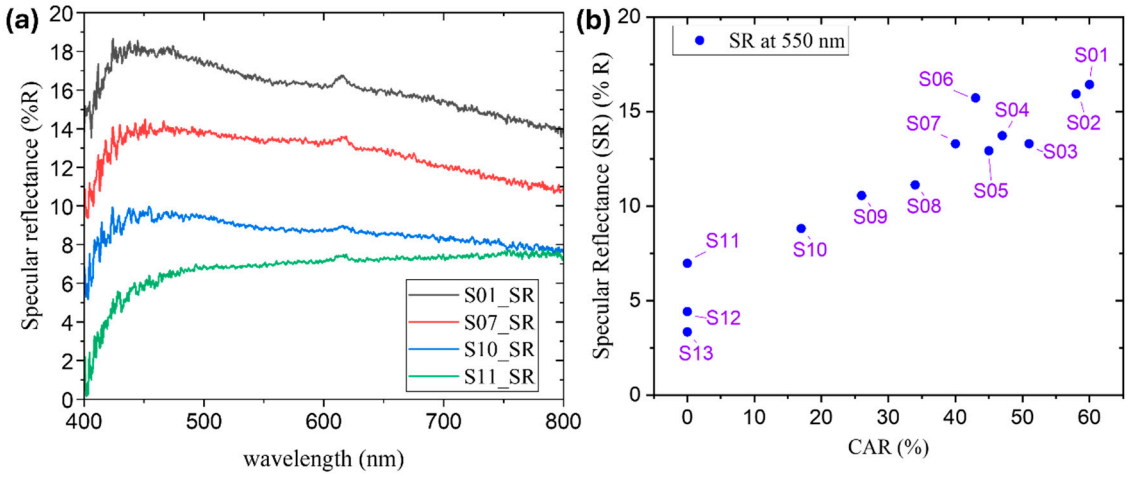

Figure 5. (a) Specular reflectance spectra in 400-800 nm of MWCNT-coated absorbers of S01, S07, S10, and S11 with varying cell area ratios (CAR). (b) Specular Reflectance at the wavelength of 550 nm for MWCNT-coated absorbers.

A spectrometer equipped with an integrating sphere was utilized to measure the total, diffuse, and specular reflectance of the MWCNT-coated absorbers across the visible wavelength range (400-800 nm). Figure 6 illustrates the reflectance values for total, diffuse, and specular reflections of samples S01, S07, S10, and S11. The fully coated MWCNT absorber (S11) exhibited the lowest average total reflectance of 6.3 ± 0.3% within the visible range compared to the honeycomb-structured MWCNT absorbers. The honeycomb-structured MWCNT absorber with the lowest CAR value in S10 (~17%) demonstrated a reduced total reflectance of 27.3 ± 1.5% compared to the honeycomb-structured MWCNT-coated absorbers with higher CAR values, S01, S07 with average total reflectance of 39.5 ± 5.5% and 33.4 ± 7.5%, respectively.

 doi:10.20944/preprints202409.1955.v

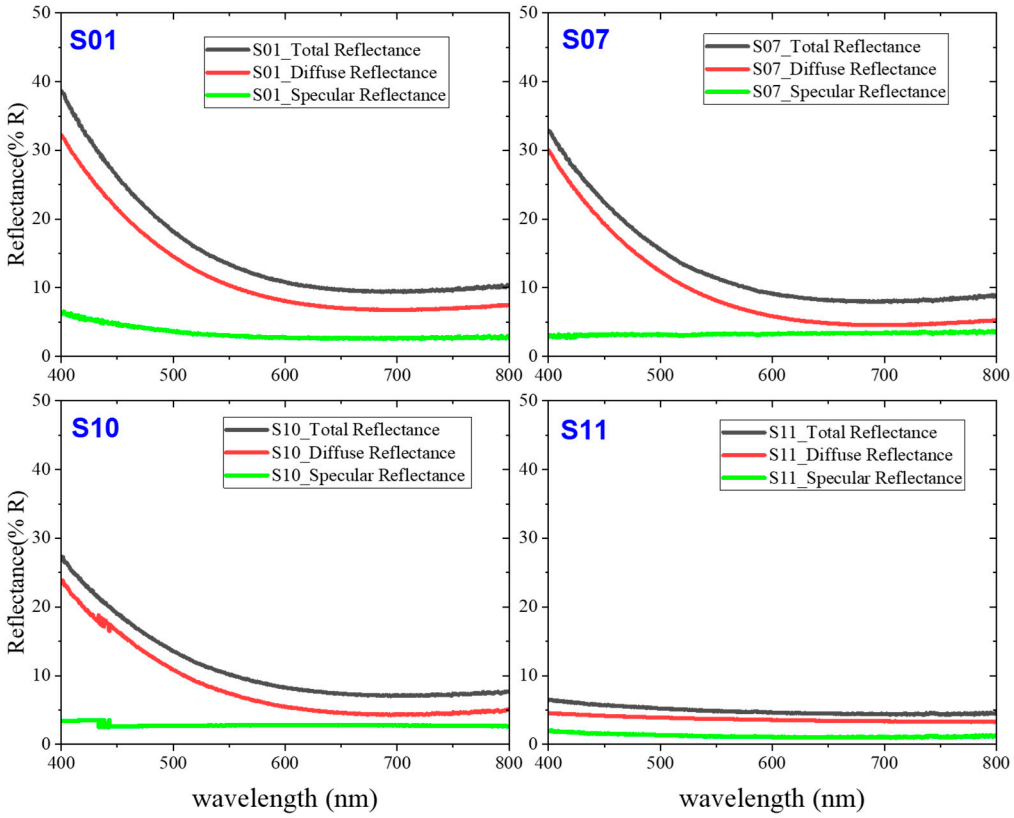

Figure 6. Total, diffuse, and specular reflectance of S01, S07, S10, and S11 samples in visible region.

Furthermore, the reflectance patterns of the MWCNT-coated absorber samples in the 934-1651 nm near-infrared wavelength range were measured, as shown in Figure 7(a). An IR spectrometer was employed to measure the reflection spectra in this range, and Eq. 1 was used to calculate the absorbance values. All samples exhibited a minor fluctuation in reflectance between 1400 and 1450 nm, attributed to the influence of the th-SiO substrate. The absorber with the most extensive honeycomb cell area ratio (CAR) structure (S01) demonstrated the lowest reflectance throughout the entire wavelength range. Reflectance generally increased as CAR decreased (S01, S07, S10). In contrast to the honeycomb structure, which exhibited a ~ 17% CAR (S10), the fully covered MWCNT absorber (S11) showed lower reflectance.

The reflectance values at 1321 nm are further reported in Figure 7(b) to investigate the reflection behavior at a selective wavelength. The absorber with complete covered (S13, 0% CAR) exhibited a reflection efficiency of 11±5.2% for the incident light at this specific wavelength. On the other hand, the honeycomb structure identified as S10 showed the lowest CAR at 17% and reflected 80.5 ± 0.9% of light at a wavelength of 1321 nm. The absorber, which featured a honeycomb structure composed of the highest CAR (60%, S01), achieved a reflection rate of 18.8 ± 3.6% at this specific wavelength. The findings indicate that lower CAR demonstrates higher reflection in the infrared spectral range. The honeycomb structures, particularly those with lower CAR, exhibit high reflectance in the infrared spectral region, highlighting potential advantages for solar thermal applications seeking to maximize thermal conversion.

 doi:10.20944/preprints202409.1955.v

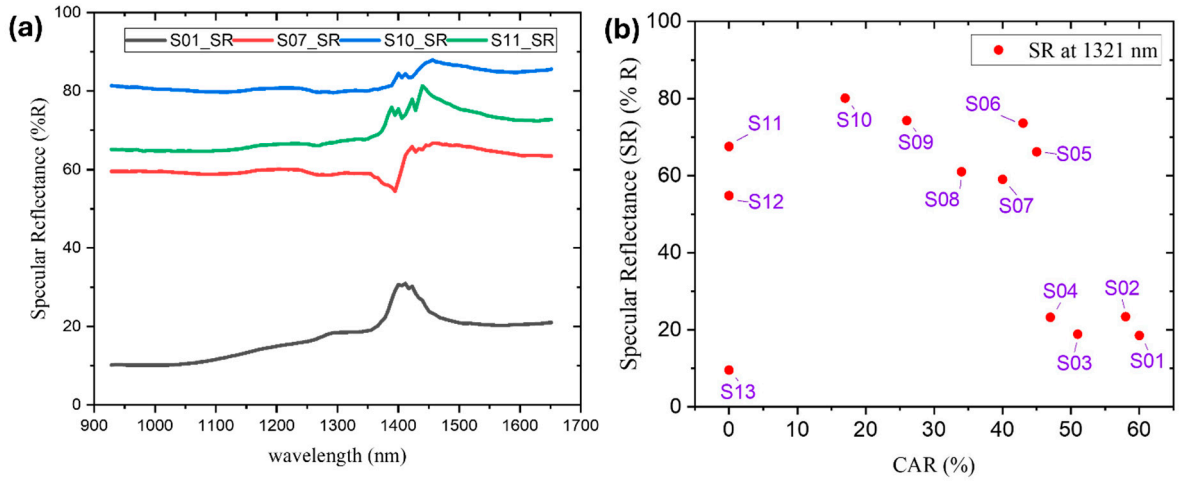

Figure 7. (a) NIR reflectance spectra of MWCNT-coated absorbers. (b) Effect of Honeycomb structured MWCNT coating's CAR on reflectance at a selective near-infrared wavelength efficiency.

The measurement of the reflection ratio at specific wavelengths, particularly the reflectance at 550 nm and 1321 nm, was performed and graphically documented in Figure 8(b). The honeycomb-structured MWCNT absorber, S10, exhibited the lowest CAR value among the samples and a comparatively lower reflection ratio of 0.11%. The CAR value and the reflection ratio exhibited a distinct linear relationship, with the sample with the highest CAR (S01) exhibiting the highest reflection ratio of 0.88%. Conversely, the absorber with a completely covered layer of MWCNT (S12) had the lowest reflectance ratio of 0.08%, distinguishing it from the other absorbers with fully covered MWCNT coatings. Prior research has also shown that the density and alignment of the MWCNTs film influence the reflectance characteristics [41,42].To further investigate the factors contributing to low reflectance, cross-sectional images of samples S11, S12, and S13 have been obtained and depicted in Figure 8(a). S11 and S12 exhibit low-density multi-walled carbon nanotube (MWCNT) films arranged horizontally, but S13 shows a thicker and densely packed MWCNT film.

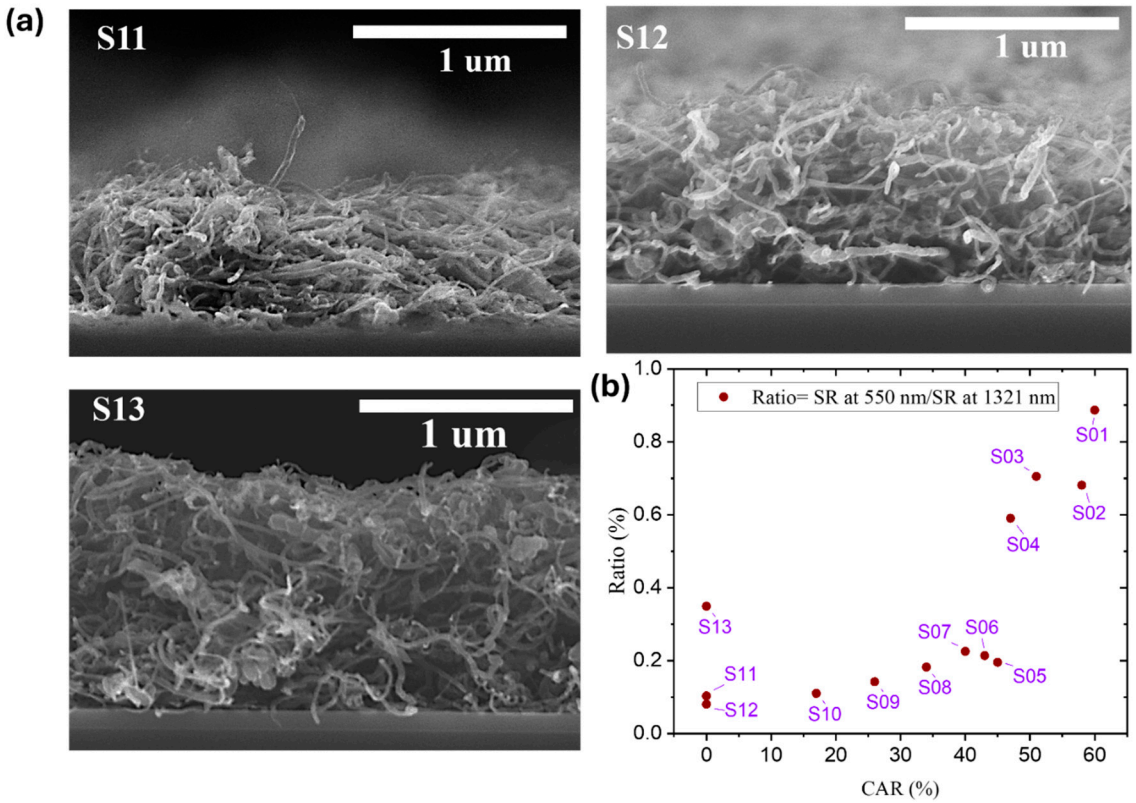

 doi:10.20944/preprints202409.1955.v

Figure 8. (a) Cross-sectional SEM images of the MWCNT coated absorbers (S11, S12, S13) (b) Reflectance ratio of MWCNT coated absorbers.

3.3. Thermal Analysis

The MWCNT-coated absorber efficiently absorbs the heat, resulting in a rise in its temperature. However, the MWCNT-coated th-SiO substrate emits heat, resulting in thermal losses. The radiative heat loss adversely affects the absorber's overall performance. The thermal conductivity of the bulk MWCNT-coated film is much higher than that of the th-SiO substrate due to its minimal thermal resistance and highly similar temperatures on both the top and bottom surfaces. The increased conductivity is due to the horizontal alignment and anisotropic characteristics of the MWCNT film [43]. As a result, MWCNT coating is the main factor influencing heat absorption and radiation. Additionally, The radiation loss from the MWCNT absorber is the primary focus of this investigation.

The MWCNT-coated solar absorbers were allowed to attain their maximum absorption temperature under saturated heating conditions by operating the halogen lamp for 300 ± 10 seconds. The lamp was turned off after the 300 ± 10 seconds heating period to allow the absorber to cool passively for 300 ± 10 seconds as it reverted to its initial resting position and temperature, as shown in Figure 9 (a-e). The temperature of all MWCNT-coated absorbers increased linearly as the illumination intensity increased. The honeycomb-structured MWCNT absorber (S10), with a 17% car value, gradually surpassed the performance of the fully covered MWCNT coated absorber (S12) at higher intensities, despite that the latter exhibited superior temperature absorption under low-intensity conditions. The observed trend has been attributed to the decreased radiative heat loss of the honeycomb structure.

The temperature decay rate for all MWCNT-coated absorbers was determined and is illustrated in Figure 9(f) during the lamp-off period. The temperature decay rates of the entirely concealed MWCNT absorber (S12) were measured to be 0.1 ± 0.02, 0.14 ± 0.05, 0.17 ± 0.07, 0.25 ± 0.14, and 0.4 ± 0.24 °C/s, respectively, exposed to irradiances of 0.04, 0.08, 0.13, 0.24, and 0.39 W/cm². Conversely, the MWCNT absorber with a honeycomb structure and a car value of ~ 17% exhibited the most significant temperature decay rates: 0.12 ± 0.02, 0.16 ± 0.04, 0.19 ± 0.08, 0.28 ± 0.14, and 0.45 ± 0.26 °C/s exposed to the same irradiances. Significantly, there was a positive correlation between an increase in CAR value and a decrease in temperature decay rate.

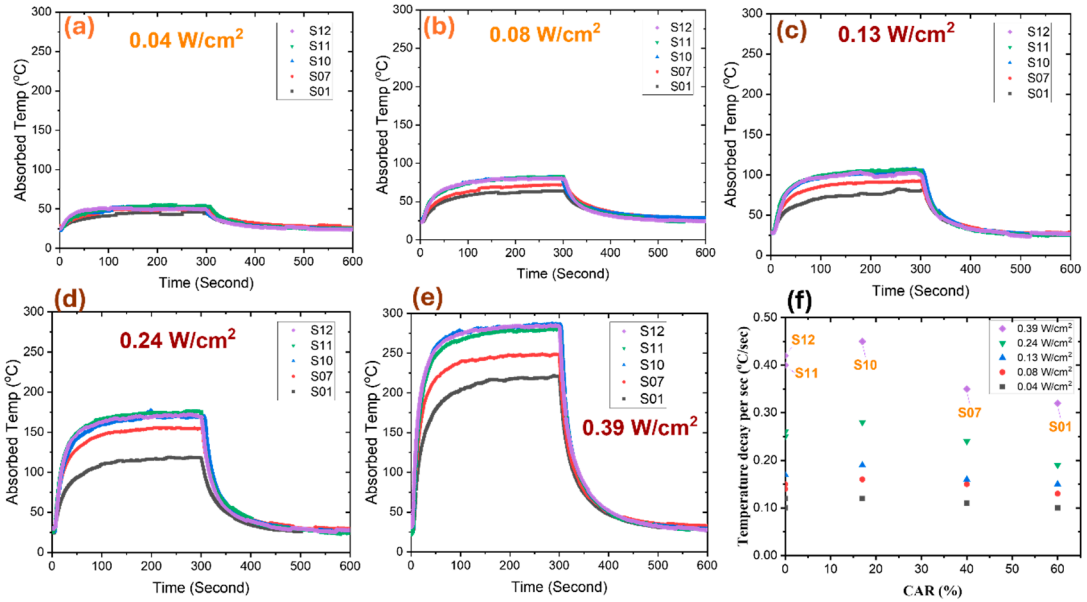

Figure 9. Temperature Absorption profile of MWCNT coated Absorber (S01, S07, S10, S11, S12) under low (a-b) and high (d-e) lamp intensities. (f) Rate of change of temperature during the lamp off under different illumination intensities.

 doi:10.20944/preprints202409.1955.v

The relationship between the maximum absorption temperature and the honeycomb structure CAR is shown in Figure 10(a). In comparison to fully covered MWCNT coated substrates (S11, S12 with 0% CAR) and absorbers with larger honeycomb structures (S01 with 60% CAR), Sample S10 absorbed the optimum temperatures of 52.5, 80.0, 105.5, 170.0, and 286.5°C under irradiances of 0.04, 0.08, 0.13, 0.24, and 0.39 W/cm², respectively. Compared to fully coated and higher car values of MWCNT absorbers, the 17% CAR of the self-organized honeycomb structured MWCNT coated absorber decreased radiation losses and increased absorption temperatures.

The solar-thermal conversion efficacy of the self-organized honeycomb-structured MWCNT absorber is confirmed by the relationship between maximum absorption temperature and the reflection ratio under varying illumination intensities, as illustrated in Figure 10(b). Under irradiances of 0.04, 0.08, 0.13, 0.24, and 0.39 W/cm², Sample S10 absorbed temperatures of 52.5, 80.0, 105.5, 170.0, and 285.5°C, respectively, with a reflection ratio of 0.11%. The S10 sample was in comparison to the entirely coated MWCNT substrates S11 (reflection ratio 0.10%) and S12 (reflection ratio 0.08%), as well as the absorber S01, which had a larger honeycomb structure and a reflection ratio of 0.88%. The results indicate that the self-organized honeycomb-structured MWCNT-coated absorber with the lowest reflection ratio of 0.11% and a lower CAR value achieved the highest absorption temperatures under varying illumination intensities, confirming its superior solar-thermal conversion performance. The results suggest it can be used in low-intensity instances, such as producing hot water for baths and showers and sterilizing medical equipment. In addition, the S10 sample's exceptional absorption is advantageous for producing electricity for low-power devices, such as sensors and small electronic equipment, and for generating potable water in coastal regions, particularly under high-intensity conditions. These applications closely align with SDG 6 [44] and SDG 7 [45].

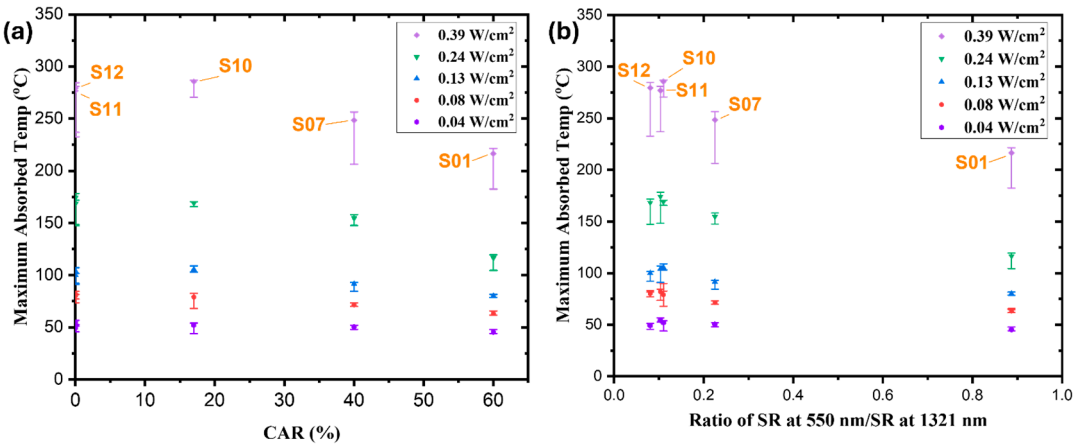

Figure 10. (a) Maximum absorbed temperature under different lamp intensities with various CARs of S01, S07, S10, S11, and S12, and (b) maximum absorbed temperature and reflectance ratio under different illumination intensities.

4. Conclusions

In summary, MWCNT-coated absorbers were prepared to utilize the drop-casting technique, resulting in a honeycomb structure with varying cell area ratios. The optical properties of the fully coated MWCNT absorbers and the obtained structures were examined. The concentration of the MWCNT solution in the deposition process was regulated using the EtOH solution to form self-organized honeycomb structures on thermal CVD SiO/Si substrates with well-controlled cell area ratios ranging from ~ 60% to 17%.

Reflectance spectra were analyzed in both visible (400-800 nm) and near-infrared (934-1651 nm) wavelength ranges. MWCNT absorbers that were utterly covered demonstrated the lowest reflection throughout the visible spectrum. However, MWCNT coatings with a honeycomb structure with a CAR value of ~17% exhibited a significant equilibrium: it maintained a reflection rate of 8.4 ± 0.8% in the visible range, specifically at the wavelength of 550 nm, which is crucial for solar energy harvesting

while exhibiting 80.5 ± 0.9% reflectance in the 1321 nm wavelength. The reflection ratio between 550 nm and 1321 nm was the linear relationship with CAR, with the lowest CAR value displaying the lowest ratio. This feature potentially increased thermal conversion efficiency by reducing infrared losses.

Furthermore, the solar thermal performance of MWCNT-coated absorbers under varying irradiance intensities, ranging from low (0.04 - 0.08 W/cm²) to high (0.13 - 0.39 W/cm²) was evaluated. The investigation showed that the honeycomb-structured MWCNT coating with a ~17% CAR performed exceptionally well at all measured intensities, reaching the maximum absorption temperatures (ranging from 52.5 to 285.5°C) as the irradiance increased. MWCNT coated absorber with ~17% CAR exhibited the highest temperature absorption compared to the fully covered MWCNT absorber and higher CAR value of honeycomb structured MWCNT coated absorber. In addition, the study found a direct relationship between the reflection ratio and the efficiency of temperature absorption at different levels of illumination intensities.

This research highlights the substantial potential for the large-scale production of cost-effective solar thermal absorbers by applying optimized honeycomb-structured MWCNT-coated absorbers. The prospective applications of these absorbers, particularly those with a ~17% CAR value, are offered by their superior performance in various solar thermal technologies.

Author Contributions: Conceptualization, S.I. and H.F.; methodology, S.I. and H.F.; validation, H.F.; investigation, S.I. and H.F.; writing—original draft preparation, S.I.; writing—review and editing, H.F.; visualization, S.I. and H.F.; supervision, H.F. All authors have read and agreed to the published version of the manuscript.

Funding: This research received no external funding.

Data Availability Statement: All data generated or analyzed during this study are included in this published article.

Acknowledgments: The authors would like to thank Akimitsu Hatta and Taue Shuji for providing equipment for the experiment.

Conflicts of Interest: The authors declare no conflict of interest.

References

1. W. Zhou *et al.*, "High-Performance Freshwater Harvesting System by Coupling Solar Desalination and Fog Collection with Hierarchical Porous Microneedle Arrays," *Adv Funct Mater*, vol. 32, no. 28, Jul. 2022, DOI: 10.1002/adfm.202113264.
2. P. G. Struchalin, D. M. Kuzmenkov, V. S. Yunin, X. Wang, Y. He, and B. V. Balakin, "Hybrid Nanofluid in a Direct Absorption Solar Collector: Magnetite vs. Carbon Nanotubes Compete for Thermal Performance," *Energies (Basel)*, vol. 15, no. 5, Mar. 2022, DOI: 10.3390/en15051604.
3. X. Liu *et al.*, "Biomass-based phase change material gels demonstrating solar-thermal conversion and thermal energy storage for thermoelectric power generation and personal thermal management," *Solar Energy*, vol. 239, pp. 307–318, Jun. 2022, DOI: 10.1016/j.solener.2022.05.004.
4. J. R. Werber, C. O. Osuji, and M. Elimelech, "Materials for next-generation desalination and water purification membranes," Apr. 05, 2016, *Nature Publishing Group*. DOI: 10.1038/natrevmats.2016.18.
5. F. Ren *et al.*, "Hydrophilicity regulation of carbon nanotubes as phase-change materials for thermal energy storage," *Journal of Materials Research and Technology*, vol. 30, pp. 1482–1489, May 2024, DOI: 10.1016/j.jmrt.2024.03.173.
6. J. Zhang, C. Wang, J. Shi, D. Wei, H. Zhao, and C. Ma, "Solar Selective Absorber for Emerging Sustainable Applications," *Advanced Energy and Sustainability Research*, vol. 3, no. 3, p. 2100195, Mar. 2022, DOI: 10.1002/aesr.202100195.
7. S. Yamashita, "Nonlinear optics in carbon nanotube, graphene, and related 2D materials," *APL Photonics*, vol. 4, no. 3, Mar. 2019, DOI: 10.1063/1.5051796.
8. D. J. Yang, S. G. Wang, Q. Zhang, P. J. Sellin, and G. Chen, "Thermal and electrical transport in multi-walled carbon nanotubes," *Physics Letters, Section A: General, Atomic and Solid State Physics*, vol. 329, no. 3, pp. 207–213, Aug. 2004, DOI: 10.1016/j.physleta.2004.05.070.
9. J.-P. Salvetat *et al.*, "Mechanical properties of carbon nanotubes," *Appl. Phys. A*, vol. 69, pp. 255–260, 1999, DOI: 10.1007/s003399900114.
10. S. Iijima, "Helical microtubules of graphitic carbon," *Nature*, vol. 354, no. 6348, pp. 56–58, Nov. 1991, DOI: 10.1038/354056a0.

11. J. Lehman, C. Yung, N. Tomlin, D. Conklin, and M. Stephens, "Carbon nanotube-based black coatings," *Appl Phys Rev*, vol. 5, no. 1, Mar. 2018, DOI: 10.1063/1.5009190.
12. P. V. Mane, R. M. Rego, P. L. Yap, D. Losic, and M. D. Kurkuri, "Unveiling cutting-edge advances in high surface area porous materials for the efficient removal of toxic metal ions from water," Dec. 01, 2024, *Elsevier Ltd*. DOI: 10.1016/j.pmatsci.2024.101314.
13. T. Zheng *et al.*, "Self-assembled multi-layered hexagonal-like MWCNTs/MnF2/CoO nanocomposite with enhanced electromagnetic wave absorption," *Carbon N Y*, vol. 186, pp. 262–272, Jan. 2022, DOI: 10.1016/j.carbon.2021.10.025.
14. A. Kumar Sharma, P. Kumar Jain, R. Vyas, V. Mathur, and V. Kumar Jain, "Study of thermal stability and dielectric behavior of PANI/MWCNT nanocomposite," in *Materials Today: Proceedings*, Elsevier Ltd, Sep. 2021, pp. 1259–1262. DOI: 10.1016/j.matpr.2020.08.235.
15. Y. Vinetsky, J. Jambu, D. Mandler, and S. Magdassi, "Cnt-based solar thermal coatings: Absorptance vs. emittance," *Coatings*, vol. 10, no. 11, pp. 1–12, Nov. 2020, DOI: 10.3390/coatings10111101.
16. T. Yang, H. Lin, K. Te Lin, and B. Jia, "Carbon-based absorbers for solar evaporation: Steam generation and beyond," Sep. 01, 2020, *Elsevier B.V.* DOI: 10.1016/j.susmat.2020.e00182.
17. Y. Jin *et al.*, "Spray coating of a perfect absorber based on carbon nanotube multiscale composites," *Carbon N Y*, vol. 178, pp. 616–624, Jun. 2021, DOI: 10.1016/j.carbon.2021.03.019.
18. X. Liu, Z. Liu, D. Devadutta Mishra, Z. Chen, J. Zhao, and C. Hu, "Evaporation rate far beyond the input solar energy limit enabled by introducing convective flow," *Chemical Engineering Journal*, vol. 429, Feb. 2022, DOI: 10.1016/j.cej.2021.132335.
19. R. J. Pan *et al.*, "Peak-like three-dimensional CoFe2O4/carbon nanotube decorated bamboo fabrics for simultaneous solar-thermal evaporation of water and photocatalytic degradation of bisphenol A," *J Mater Sci Technol*, vol. 179, pp. 40–49, Apr. 2024, DOI: 10.1016/j.jmst.2023.08.045.
20. M. Yu *et al.*, "Preparation of ultra-black film with good resistance to wiping based on a typical forest structure," *Prog Org Coat*, vol. 195, Oct. 2024, DOI: 10.1016/j.porgcoat.2024.108638.
21. P. M. Martinez, V. A. Pozdin, A. Papadimitratos, W. Holmes, F. Hassanipour, and A. A. Zakhidov, "Dual use of carbon nanotube selective coatings in evacuated tube solar collectors," *Carbon N Y*, vol. 119, pp. 133–141, Aug. 2017, DOI: 10.1016/j.carbon.2017.04.026.
22. J. Udorn, A. Hatta, and H. Furuta, "Carbon nanotube (CNT) honeycomb cell area-dependent optical reflectance," *Nanomaterials*, vol. 6, no. 11, Nov. 2016, DOI: 10.3390/nano6110202.
23. S. Hong, Y. Shi, R. Li, C. Zhang, Y. Jin, and P. Wang, "Nature-Inspired, 3D Origami Solar Steam Generator toward Near Full Utilization of Solar Energy," *ACS Appl Mater Interfaces*, vol. 10, no. 34, pp. 28517–28524, Aug. 2018, DOI: 10.1021/acsami.8b07150.
24. F. Kiani, F. Sterl, T. V. Tsoulos, K. Weber, H. Giessen, and G. Tagliabue, "Ultra-broadband and omnidirectional perfect absorber based on copper nanowire/carbon nanotube hierarchical structure," *ACS Photonics*, vol. 7, no. 2, pp. 366–374, Feb. 2020, DOI: 10.1021/acsphotonics.9b01658.
25. V. Ghai, H. Singh, and P. K. Agnihotri, "Structure Dependent Broadband Optical Absorption in Carbon Nanotubes," *ACS Applied Optical Materials*, vol. 1, no. 1, pp. 252–260, Jan. 2023, DOI: 10.1021/acsaom.2c00047.
26. A. Pander, T. Onishi, A. Hatta, and H. Furuta, "Fabrication of Self-Assembling Carbon Nanotube Forest Fishnet Metamaterials," *Nanomaterials*, vol. 12, no. 3, Feb. 2022, DOI: 10.3390/nano12030464.
27. Y. Huang, L. Zhu, Q. Huang, and Z. C. He, "Effect of carbon nanotubes and TiN nanoparticles on light absorption property of nanostructured carbon-based coatings fabricated by high-voltage electrostatic spraying technique," *Opt Mater (Amst)*, vol. 150, Apr. 2024, DOI: 10.1016/j.optmat.2024.115172.
28. J. Jiang, H. Jiang, Y. Xu, M. Chen, and L. Ai, "Janus Co@C/NCNT photothermal membrane with multiple optical absorption for highly efficient solar water evaporation and wastewater purification," *Colloids Surf A Physicochem Eng Asp*, vol. 647, Aug. 2022, DOI: 10.1016/j.colsurfa.2022.128960.
29. M. He, H. Liu, L. Wang, X. Qin, and J. Yu, "One-step fabrication of a stretchable and anti-oil-fouling nanofiber membrane for solar steam generation," *Mater Chem Front*, vol. 5, no. 9, pp. 3673–3680, May 2021, DOI: 10.1039/d1qm00101a.
30. M. Jin *et al.*, "Hierarchically Designed Three-Dimensional Composite Structure on a Cellulose-Based Solar Steam Generator," *ACS Appl Mater Interfaces*, vol. 14, no. 10, pp. 12284–12294, Mar. 2022, DOI: 10.1021/acsami.1c24847.
31. Q. Li *et al.*, "Porous Ni/CNTs composite membrane as solar absorber for highly efficient solar steam generation," *Solar Energy Materials and Solar Cells*, vol. 243, Aug. 2022, DOI: 10.1016/j.solmat.2022.111815.
32. S. Zhang *et al.*, "Multiscale Preparation of Graphene Oxide/Carbon Nanotube-Based Membrane Evaporators by a Spray Method for Efficient Solar Steam Generation," *ACS Appl Nano Mater*, May 2022, DOI: 10.1021/acsanm.2c01122.
33. D. Wang *et al.*, "Hanging Photothermal Fabric Based on Polyaniline/Carbon Nanotubes for Efficient Solar Water Evaporation," *ACS Omega*, vol. 8, no. 47, pp. 44659–44666, Nov. 2023, DOI: 10.1021/acsomega.3c05332.

34. T. Saleh *et al.*, "Transforming carbon nanotube forest from darkest absorber to reflective mirror," *Appl Phys Lett*, vol. 101, no. 6, Aug. 2012, DOI: 10.1063/1.4744429.
35. Z. Han, Z. Jiao, S. Niu, and L. Ren, "Ascendant bioinspired antireflective materials: Opportunities and challenges coexist," Jun. 01, 2019, *Elsevier Ltd*. DOI: 10.1016/j.pmatsci.2019.01.004.
36. Y. Qiu, M. Lee, J. Chen, and Q. Zhang, "Effect of light intensity on solar-driven interfacial steam generation," Dec. 28, 2021, *Royal Society of Chemistry*. DOI: 10.1039/d1nr06410j.
37. S. Islam and H. Furuta, "Recent Development of Carbon-Nanotube-Based Solar Heat Absorption Devices and Their Application," Nov. 01, 2022, *MDPI*. DOI: 10.3390/nano12213871.
38. M. Zhang, S. Inoue, and Y. Matsumura, "Difference in Gas-Sensing behavior of Multi-walled carbon Nanotube-Paper-Based gas sensor to polar and non-Polar organic solvents," *Chem Phys Lett*, vol. 798, Jul. 2022, DOI: 10.1016/j.cplett.2022.139596.
39. M. Łojkowski, A. Chlanda, E. Choińska, and W. Swieszkowski, "Water vapor induced self-assembly of islands/honeycomb structure by secondary phase separation in polystyrene solution with bimodal molecular weight distribution," *Sci Rep*, vol. 11, no. 1, Dec. 2021, DOI: 10.1038/s41598-021-92594-1.
40. J. A. Maroto, V. Pérez-Mũuzuri, and M. S. Romero-Cano, "Introductory analysis of Bénard-Marangoni convection," *Eur J Phys*, vol. 28, no. 2, pp. 311–320, Mar. 2007, DOI: 10.1088/0143-0807/28/2/016.
41. B. D. Wood, J. S. Dyer, V. A. Thurgood, N. A. Tomlin, J. H. Lehman, and T.-C. Shen, "Optical reflection and absorption of carbon nanotube forest films on substrates," *J Appl Phys*, vol. 118, no. 1, p. 013106, Jul. 2015, DOI: 10.1063/1.4923390.
42. K. Nomura, Y. Sawada, H. Nishimori, A. Hatta, and H. Furuta, "Basic Research on CNT Structures for the Solar Water Heater Applications," *JSAP Annual Meetings Extended Abstracts*, vol. 2021.1, p. 2790, 2021, DOI: 10.11470/jsapmeeting.2021.1.0_2790.
43. B. Kumanek and D. Janas, "Thermal conductivity of carbon nanotube networks: a review," May 30, 2019, *Springer New York LLC*. DOI: 10.1007/s10853-019-03368-0.
44. V. Herrera, "Reconciling global aspirations and local realities: Challenges facing the Sustainable Development Goals for water and sanitation," *World Dev*, vol. 118, pp. 106–117, Jun. 2019, doi: 10.1016/j.worlddev.2019.02.009.
45. N. Manoj Kumar, S. S. Chopra, A. A. Chand, R. M. Elavarasan, and G. M. Shafiullah, "Hybrid renewable energy microgrid for a residential community: A techno-economic and environmental perspective in the context of the SDG7," *Sustainability (Switzerland)*, vol. 12, no. 10, May 2020, DOI: 10.3390/SU12103944.